


 Cite this: *Chem. Commun.*, 2019, 55, 14950

 Received 14th October 2019,  
 Accepted 15th November 2019

DOI: 10.1039/c9cc08070h

rsc.li/chemcomm

## Hydrophobicity and CH/ $\pi$ -interaction-driven self-assembly of amphiphilic aromatic hydrocarbons into nanosheets†

 Tsuyoshi Nishikawa,<sup>a</sup> Hiroki Narita,<sup>a</sup> Soichiro Ogi,<sup>b</sup> Yoshikatsu Sato<sup>b</sup> and Shigehiro Yamaguchi<sup>b\*</sup>

**The hydrophobicity and CH/ $\pi$ -interaction-driven self-assembly of an amphiphile that contains a biphenylanthracene group furnishes two-dimensional aggregates in dilute aqueous solution. A windmill-shaped molecular packing structure that arises from multiple intermolecular CH/ $\pi$  interactions of the aromatic hydrocarbons is the key motif for the self-assembly into micrometer-scale nanosheets.**

Two-dimensional (2-D) materials, represented by graphene and metal oxides, have recently received increasing attention due to their various functions derived from their dimensionality, which include *e.g.*, a high charge-carrier mobility, effective adsorption of target molecules, and a large surface area that enables the accumulation of various functional groups.<sup>1</sup> The use of such materials in aqueous media is highly attractive, especially with regard to constructing bio-adaptive functional materials.<sup>2</sup> For example, the catalytic activity of enzymes can be improved by fixation on graphene oxide.<sup>3</sup>

In order to promote further development in this field, it is important to establish a methodology for the efficient preparation of self-standing and well-defined 2-D structures. To this end, the supramolecular approach represents an attractive strategy due to the high modularity and tunability of organic molecules and their self-assembling properties. While ionic interactions and hydrogen bonding have been widely used to induce self-assembly in organic media,<sup>4,5</sup> these interactions are substantially perturbed by hydration in aqueous media. In contrast, the use of hydrophobic effects may be an effective way to induce self-assembly in aqueous solvents. Recent research has demonstrated that amphiphiles that consist of hydrophobic

$\pi$ -skeletons and hydrophilic chains self-assemble into self-standing sheet-like aggregates.<sup>6–9</sup> However, the structural requirements of amphiphiles for a self-assembly into self-standing 2-D organic materials with well-defined packing structures have not been fully established.

In this regard, CH/ $\pi$  interactions, a type of hydrogen bond, can be a useful means to control the packing mode in the self-assembled structure.<sup>10</sup> While an individual CH/ $\pi$  interaction is insufficient to overcome the entropic cost of arranging  $\pi$ -skeletons, multiple CH/ $\pi$  interactions may cooperatively facilitate such an alignment, as evident in the crystal structures of aromatic hydrocarbons.<sup>11</sup> Anthracene is a representative example in which the CH/ $\pi$  interactions between the edge C(sp<sup>2</sup>)-H bonds and the anthracene  $\pi$ -planes give rise to its herringbone packing.<sup>12</sup> Such CH/ $\pi$  hydrogen bonds would presumably also work in water as the bond energy is derived mostly from the dispersion force. Furthermore, orthogonal CH/ $\pi$  interaction can contribute to constructing higher dimensional structures such as 2-D sheets in comparison with the  $\pi$ - $\pi$  interaction leading to 1-D arrangement of molecules. Accordingly, we envisioned that an anthracene-based amphiphile could potentially self-assemble into well-defined structures (*e.g.*, sheet-like aggregates) in aqueous media based on the synergy of hydrophobicity and CH/ $\pi$  interactions (Fig. 1).

Herein, we report that amphiphiles that contain a hydrophobic biphenylanthracene group and a hydrophilic ethylene oxide chain afford sheet-like aggregates at concentrations as low as  $5 \times 10^{-6}$  M in aqueous solvents. The key design feature is the orthogonal arrangement of the anthracene and the biphenylene moiety, which have comparable skeletal lengths to each other, thereby being suited to form a windmill-shaped packing motif through multi-fold intermolecular CH/ $\pi$  interaction between anthracene and biphenylene groups. The importance of CH/ $\pi$  interaction for guiding the self-assembly into 2-D aggregates is discussed by comparisons with self-assembling behavior of several other relevant compounds.

Initially, we investigated the self-assembling behavior of an anthracene bearing a hydrophilic ethylene oxide chain 1

<sup>a</sup> Department of Chemistry, Graduate School of Science, Nagoya University, Furo, Chikusa, Nagoya, 464-8602, Japan. E-mail: yamaguchi@chem.nagoya-u.ac.jp

<sup>b</sup> Institute of Transformative Bio-Molecules (WPI-ITbM), Nagoya University, Furo, Chikusa, Nagoya, 464-8602, Japan

† Electronic supplementary information (ESI) available: Experimental procedures, spectral data, details of computational studies, and crystallographic data for 3, 9-([1,1'-biphenyl]-4-yl)anthracene, and 6. CCDC 1824326, 1953600 and 1953601. For ESI and crystallographic data in CIF or other electronic format see DOI: 10.1039/c9cc08070h

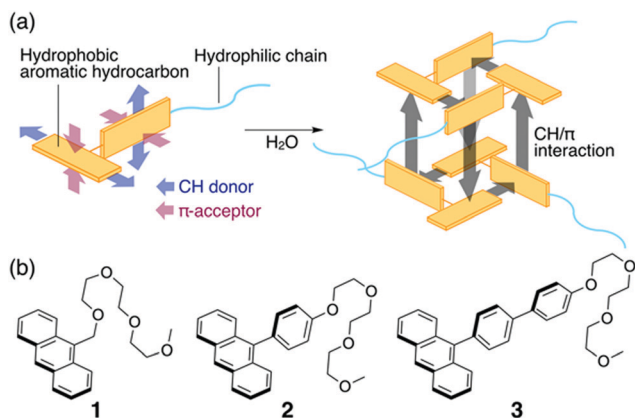


**Fig. 1** (a) Schematic representation of the synergy between hydrophobicity and CH/ $\pi$ -interactions that leads to the self-assembly of amphiphilic aromatic hydrocarbons and (b) chemical structures of **1–3**.

in aqueous media. For the preparation of an aggregated sample, a 1-propanol (1-PrOH) solution of **1** ( $5 \times 10^{-5}$  M) was added to distilled water until the water content reached 90 vol% with a total concentration of  $5 \times 10^{-6}$  M. The solution was shaken and then allowed to stand at room temperature ( $\sim 20^\circ\text{C}$ ) for 12 h. A small portion of the solution was placed onto a carbon-coated copper grid and examined by transmission electron microscopy (TEM) (Fig. S1, ESI $^\dagger$ ). A TEM image of this sample showed only the formation of unstructured aggregates of **1** (Fig. 2a). Even at a concentration of  $5 \times 10^{-4}$  M, the morphology of **1** was particulate, suggesting that its molecular structure is not suitable for self-assembly into higher-order structures (Fig. S2 and S3, ESI $^\dagger$ ).

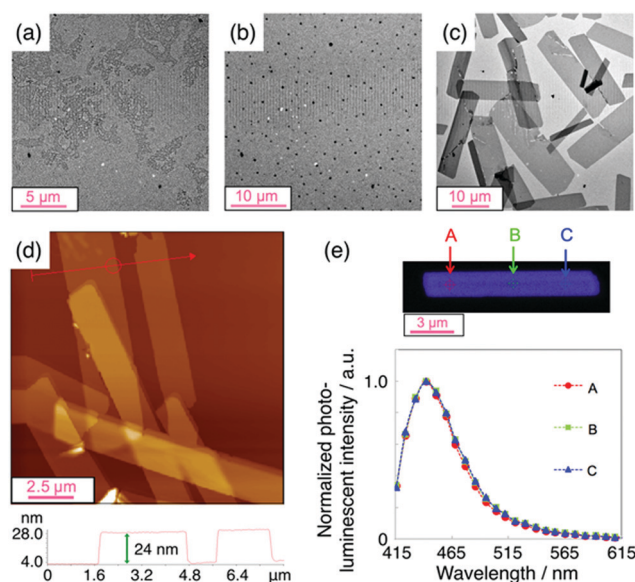


**Fig. 2** (a–c) TEM images of (a) **1**, (b) **2**, and (c) **3** in the aggregated states; (d) AFM height image of sheet-like aggregates obtained from a solution of **3** in 10/90 (v/v) 1-PrOH/H<sub>2</sub>O together with a cross-section analysis corresponding to the red arrow; (e) result of the spectral imaging and normalized fluorescent spectra at positions A, B, and C of **3**.

Consequently, we introduced *p*-phenylene or 4,4'-biphenylene units between the anthracene and the hydrophilic chain of **1** (**2** and **3** in Fig. 1b) in order to induce the formation of multiple CH/ $\pi$  interactions. Solutions of **2** and **3** in 10/90 (v/v) 1-PrOH/H<sub>2</sub>O with a total concentration of  $5 \times 10^{-6}$  M were prepared in the same manner as that of **1**. Whereas phenylene-containing **2** formed particles with a size of less than 1  $\mu\text{m}$  (Fig. 2b), biphenylene-containing **3** self-assembled into sheet-like aggregates with a size on the  $\mu\text{m}$  scale (Fig. 2c). Since **3** is molecularly dispersed at  $5 \times 10^{-6}$  M in pure 1-PrOH, the hydrophobicity of the biphenylanthracene moiety is assumed to induce the self-assembly at such a low concentration in the presence of water. A TEM image of a freshly prepared sample of **3** revealed the presence of unstructured aggregates, which were transformed into sheet-like aggregates after standing for several hours (Fig. S4, ESI $^\dagger$ ). Monitoring the time-dependent transformation by UV-vis absorption spectroscopy revealed that this process is completed after 12 h (Fig. S5, ESI $^\dagger$ ).

The morphology of the sheet-like aggregates of **3** was further studied by atomic force microscopy (AFM). A sample was prepared by drop casting a 10/90 (v/v) 1-PrOH/H<sub>2</sub>O solution of **3** on a silicon wafer. An AFM image confirmed the sheet-like morphology with a  $\mu\text{m}$ -scale lateral size similar to that observed by TEM (Fig. 2d). Importantly, the thicknesses of the sheets ( $27 \pm 6$  nm) is by two to three orders of magnitude lower than the lateral size, and this pronounced aspect ratio strongly suggests the presence of 2-D aggregates.

The sheet morphology for the aggregates of **3** was also confirmed by fluorescence microscopy. A sample was prepared by drop-casting a 10/90 (v/v) 1-PrOH/H<sub>2</sub>O solution of **3** on a glass substrate in a manner similar to that of the AFM sample. The 2-D sheet exhibited blue emission, and several individual spectra were directly recorded at different points on the aggregates by the spectral imaging using a confocal laser microscope (Fig. 2e). The thus obtained spectra were essentially identical, indicating that the morphology of the 2-D sheets is uniform (Fig. S6, ESI $^\dagger$ ). It should be noted that an identical 2-D-sheet morphology was observed on the different substrates such as carbon films, silicon wafers, and glass plates. These microscopic results indicate that the self-assembly of **3** into sheets occurs in solution prior to the drop-casting onto substrates and not on the surface of the substrates.

The high propensity of **3** to form 2-D nanosheets should be related to its packing structure. To gain insight into the intermolecular interactions between the biphenylanthracene moieties in the aggregates, X-ray powder diffraction (XRPD) measurements were carried out (Fig. 3). An aggregate sample was prepared at a concentration of  $5 \times 10^{-5}$  M in 10/90 (v/v) 1-PrOH/H<sub>2</sub>O. TEM and AFM images confirmed that the thus obtained aggregates exhibit a morphology that is similar to those prepared at  $5 \times 10^{-6}$  M (Fig. S7 and S8, ESI $^\dagger$ ). The XRPD measurements on the nanosheets, collected by freeze-drying, showed sharp peaks, which is indicative of a well-ordered molecular packing of **3** in the aggregated state (Fig. 3a).

To determine the molecular packing, we also tried to prepare a single crystal for a single-crystal X-ray diffraction analysis by slowly

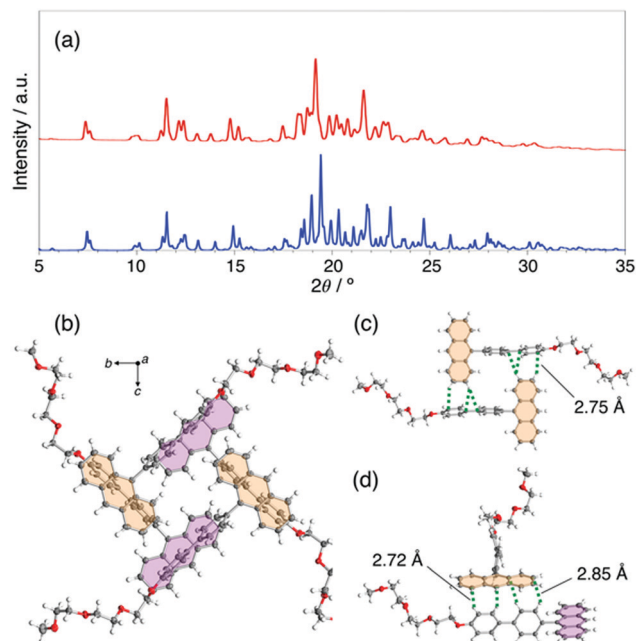


**Fig. 3** (a) XRPD pattern of sheet-like aggregates (red) and a single-crystal XRD pattern (blue) of **3**; (b) windmill-shaped molecular packing in sheet-like aggregates of **3**; (c and d) two types of intermolecular CH/ $\pi$  interactions between the anthracene and biphenyl units of **3**.

cooling a hot solution of **3** in 1-PrOH to ambient temperature. The XRD pattern of the single crystal matched well with that of the nanosheets obtained from the solution in 10/90 (v/v) 1-PrOH/H<sub>2</sub>O. Specifically, the single crystal and the sheet-like aggregates exhibit an essentially identical packing motif and the crystallographic data can be used for a discussion of the molecular packing in the nanosheets.<sup>13</sup>

The X-ray crystallographic analysis of **3** revealed a packing structure that is characterized by a symmetric windmill-shaped alignment of four molecules (Fig. 3b), while the hydrophilic ethylene oxide chains are oriented outward with respect to the windmill core. Notably, the biphenylanthracene moieties of the four molecules are close to each other and engage in two kinds of intermolecular CH/ $\pi$  interactions. Firstly, the C–H bonds at the 2,3-positions of the anthracene point toward the biphenyl benzene plane of an adjacent molecule with a nonbonded H...C distance of  $\sim 2.75$  Å, which demonstrates that the anthracene and biphenyl moieties act as hydrogen-donor and -acceptor, respectively (Fig. 3c and Fig. S9a, ESI<sup>†</sup>). This interaction is responsible for the anti-parallel orientation of two molecules. Secondly, CH/ $\pi$  interactions also occur in a vertical direction between the hydrogen atoms of the biphenylene moiety and the anthracene plane of an adjacent molecule with nonbonding H...C distances of  $\sim 2.8$  Å (Fig. 3d and Fig. S9b, ESI<sup>†</sup>).<sup>10c</sup> Importantly, the biphenyl moiety adopts a coplanar conformation with a dihedral angle of  $27.0^\circ$ , which renders the CH/ $\pi$  interaction effective. The packing structure is fundamentally different from that of 9-([1,1'-biphenyl]-4-yl)anthracene, in which the C–H bonds at the 4,5,10-positions of the anthracene are pointed toward the anthracene plane of an adjacent

molecule (Fig. S10, ESI<sup>†</sup>). In addition, the biphenyl moiety exhibits a dihedral angle of  $37.6^\circ$ . This comparison clearly suggests that the amphiphilic structure is essential for inducing the windmill-shaped alignment of the biphenylanthracene group. A nature of rigidity and subsequent high crystallinity of the aromatic moiety would contribute to segregation from the flexible ethylene oxide chains and efficient formation of the intermolecular CH/ $\pi$  interactions.<sup>14</sup>

A key feature to realize the crystalline growth into sheet-like aggregates is the precise design of the oligomeric core packing structure.<sup>9,14</sup> In this regard, our design relies on the multiple intermolecular CH/ $\pi$  interactions between the anthracene and biphenyl moieties. It is reasonable to assume that the presence of hydrophilic chains on the surface of the sheets decreases the surface free energy of hydrophobic aggregates toward highly polar solvents. Indeed, XRD analyses revealed that a line cut along the out-of-plane direction exhibits the (010) plane, which is parallel to the *a* axis (Fig. S11, ESI<sup>†</sup>). Namely, the windmill-shaped oligomers are arranged along the in-plane direction of nanosheets *via* the CH/ $\pi$  interactions between the biphenylene moiety and the anthracene plane of adjacent molecules. Consequently, the thickness of a monolayer is  $\sim 2.6$  nm, which suggests that the sheets shown in Fig. 2d consists of 8–12 layers of the unit cell.

Finally, the aggregate morphology of reference compounds **4–6** was compared to that of **3** in order to better understand the impact of the CH/ $\pi$  interactions on the hydrophobicity and the CH/ $\pi$ -interaction-driven self-assembly into nanosheets (Fig. 4a and Fig. S12, ESI<sup>†</sup>). TEM images revealed that amphiphile **4**, which contains an anthracene inserted between a biphenylene moiety, did not form a sheet-like structure under the conditions used for **3**. In addition, amphiphile **5**, in which bulky isopropyl groups were introduced at the *o,o*-positions of the phenylene group to prevent CH/ $\pi$  interactions, only produced undefined

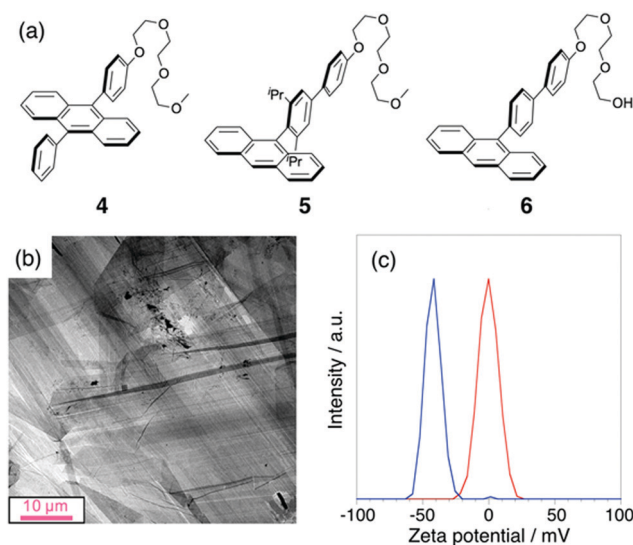


**Fig. 4** (a) Chemical structures of **4–6**; (b) TEM image of **6** in the aggregated state; (c) zeta potential distributions of aggregated **3** (red line) and **6** (blue line).

aggregates. These results confirm that the CH/ $\pi$  interactions between the biphenyl and anthracene moieties in **3** are essential to promote the observed 2-D self-assembling behavior.

On the other hand, replacement of the methoxy group at the end of the hydrophilic chain with a hydroxy group in **6** afforded belt-like aggregates, which hierarchically assemble into sheet-like aggregates (Fig. 4b and Fig. S13, S14, ESI<sup>†</sup>). Notably, the thickness of the aggregates obtained from a solution at  $5 \times 10^{-6}$  M in 10/90 (v/v) 1-PrOH/H<sub>2</sub>O was  $\sim 3\text{--}6$  nm (Fig. S14b and c, ESI<sup>†</sup>), which is much thinner than those obtained for **3**. The XRPD pattern of the nanosheets of **6** was consistent with that observed for its single crystals, which also show a windmill-shaped packing structure that is essentially similar to that of **3** (Fig. S15 and S16, ESI<sup>†</sup>). Nanosheets of **6** exhibit negative zeta potentials (Fig. 4c), whereas the zeta potentials results imply that the surface properties of the biphenylanthracene-based nanosheets are tunable by varying the terminal group of the hydrophilic chain.

In conclusion, we have introduced biphenylanthracene as a useful motif to induce hydrophobicity and CH/ $\pi$ -interaction-driven self-assembly into nanosheets. A combination of biphenylanthracene moieties and long hydrophilic chains affords amphiphiles that are able to engage in multiple intermolecular CH/ $\pi$  interactions. The thus produced windmill-shaped packing structures effectively form sheet-like aggregates with a  $\mu\text{m}$ -scale lateral size at very low concentrations. In this molecular design, changing the terminal groups of the hydrophilic chains allows modifying the surface character of the nanosheets. Further investigations into the development of functional materials based on the two-dimensionality of the sheets are currently in progress in our laboratory.

This work was supported by Grants-in-Aid for Young Scientists (B) (KAKENHI grant JP17K14469 to S. O.) from the Japan Society for the Promotion of Science (JSPS). This work was partly supported by JSPS KAKENHI grant JP16H06280. The authors thank Prof. Takahiro Sasamori (Nagoya City Univ.), and Prof. Mao Minoura (Rikkyo Univ.), as well as Dr Masato Hirai, Dr Naoki Ando, Mr Junichi Usuba, and Mr Masahiro Hayakawa (Nagoya Univ.) for X-ray crystallographic analyses. The synchrotron X-ray crystallography experiment was performed at the BL40XU beamline of SPring-8 with the approval of the Japan Synchrotron Radiation Research Institute (JASRI; proposal 2018B1084, 2018B1275). The authors are grateful to Mr Tatsuo Hikage for XRPD measurements.

## Conflicts of interest

The authors declare the absence of any potential conflicts of interest.

## Notes and references

- (a) C. N. R. Rao, A. K. Sood, K. S. Subrahmanyam and A. Govindaraj, *Angew. Chem., Int. Ed.*, 2009, **48**, 7752–7777; (b) G. R. Bhimanapati, Z. Lin, V. Meunier, Y. Jung, J. Cha, S. Das, D. Xiao, Y. Son, M. S. Strano, V. R. Cooper, L. Liang, S. G. Louie, E. Ringe, W. Zhou, S. S. Kim, R. R. Naik, B. G. Sumpter, H. Terrones, F. Xia, Y. Wang, J. Zhu, D. Akinwande, N. Alem, J. A. Schuller, R. E. Schaak, M. Terrones and J. A. Robinson, *ACS Nano*, 2015, **9**, 11509–11539.
- (a) X. Sun, Z. Liu, K. Welscher, J. T. Robinson, A. Goodwin, S. Zaric and H. Dai, *Nano Res.*, 2008, **1**, 203–212; (b) D. Chimene, D. L. Alge and A. K. Gaharwar, *Adv. Mater.*, 2015, **27**, 7261–7284.
- (a) L. Jin, K. Yang, K. Yao, S. Zhang, H. Tao, S. T. Lee, Z. Liu and R. Peng, *ACS Nano*, 2012, **6**, 4864–4875; (b) Z. Liu, J. T. Robinson, X. Sun and H. Dai, *J. Am. Chem. Soc.*, 2008, **130**, 10876–10877.
- K. T. Nam, D. A. Shelby, P. H. Choi, A. B. Marciel, R. Chen, L. Tan, T. K. Chu, R. A. Mesch, B. C. Lee, M. D. Connolly, C. Kisielowski and R. N. Zuckermann, *Nat. Mater.*, 2010, **9**, 454–460.
- H. S. Jang, J. H. Lee, Y. S. Park, Y. O. Kim, J. Park, T. Y. Yang, K. Jin, J. Lee, S. Park, J. M. You, K. W. Jeong, A. Shin, I. S. Oh, M. K. Kwon, Y. I. Kim, H. H. Cho, H. N. Han, Y. Kim, Y. H. Chang, S. R. Paik, K. T. Nam and Y. S. Lee, *Nat. Commun.*, 2014, **5**, 3665.
- S. Ghosh, D. S. Phillips, A. Saeki and A. Ajayaghosh, *Adv. Mater.*, 2017, **29**, 1605408.
- (a) A. S. Weingarten, R. V. Kazantsev, L. C. Palmer, M. McClendon, A. R. Koltanow, A. P. S. Samuel, D. J. Kiebal, M. R. Wasielewski and S. I. Stupp, *Nat. Chem.*, 2014, **6**, 964–970; (b) R. V. Kazantsev, A. J. Dannenhoffer, A. S. Weingarten, B. T. Phelan, B. Harutyunyan, T. Aytun, A. Narayanan, D. J. Fairfield, J. Boekhoven, H. Sai, A. Senesi, P. I. O'Dogherty, L. C. Palmer, M. J. Bedzyk, M. R. Wasielewski and S. I. Stupp, *J. Am. Chem. Soc.*, 2017, **139**, 6120–6127.
- (a) E. Lee, J. K. Kim and M. Lee, *Angew. Chem., Int. Ed.*, 2009, **48**, 3657–3660; (b) H. J. Kim, T. Kim and M. Lee, *Acc. Chem. Res.*, 2011, **44**, 72–82.
- (a) M. Vybornyi, A. V. Rudnev, S. M. Langenegger, T. Wandlowski, G. Calzaferri and R. Häner, *Angew. Chem., Int. Ed.*, 2013, **52**, 11488–11493; (b) M. Vybornyi, A. Rudnev and R. Häner, *Chem. Mater.*, 2015, **27**, 1426–1431.
- (a) M. Nishio, M. Hirota and Y. Umezawa, *The CH/ $\pi$  interaction. Evidence, Nature, and Consequences*, Wiley-VCH, New York, 1998; (b) M. Nishio, Y. Umezawa, K. Honda, S. Tsuboyama and H. Suezawa, *CrystEngComm*, 2009, **11**, 1757–1788; (c) H. Suezawa, S. Ishihara, Y. Umezawa, S. Tsuboyama and M. Nishio, *Eur. J. Org. Chem.*, 2004, 4816–4822.
- (a) J. E. Anthony, *Chem. Rev.*, 2006, **106**, 5028–5048; (b) M. Nishio, Y. Umezawa, J. Fantini, M. S. Weiss and P. Chakrabarti, *Phys. Chem. Chem. Phys.*, 2014, **16**, 12648–12683.
- C. P. Brock and J. D. Dunitz, *Acta Crystallogr., Sect. B: Struct. Sci.*, 1990, **46**, 795–806.
- S. Saito, K. Nakakura and S. Yamaguchi, *Angew. Chem., Int. Ed.*, 2012, **51**, 714–717.
- (a) Y. Zheng, H. Zhou, D. Liu, G. Floudas, M. Wagner, K. Koynov, M. Mezger, H. J. Butt and T. Ikeda, *Angew. Chem., Int. Ed.*, 2013, **52**, 4845–4848; (b) T. Ikeda, *Langmuir*, 2015, **31**, 667–673.